Received: 28 February 2024 | Revised: 17 June 2024 | Accepted: 13 July 2024

DOI: 10.1002/num.23132

RESEARCH ARTICLE

WILEY

Partitioning method for the finite element approximation of a 3D fluid-2D plate interaction system

Pelin G. Geredeli | **Hemanta Kunwar** | **Hyesuk Lee**

School of Mathematical and Statistical Sciences, Clemson University, Clemson, South Carolina, USA

Correspondence
Hyesuk Lee, School of Mathematical and Statistical Sciences, Clemson University, Clemson, SC 29634-0975, USA.
Email: hklee@clemson.edu

Funding information
NSF, Grant/Award Numbers: DMS-2348312, DMS-2207971

Abstract

We consider the finite element approximation of a coupled fluid-structure interaction (FSI) system, which comprises a three-dimensional (3D) Stokes flow and a two-dimensional (2D) fourth-order Euler–Bernoulli or Kirchhoff plate. The interaction of these parabolic and hyperbolic partial differential equations (PDE) occurs at the boundary interface which is assumed to be fixed. The vertical displacement of the plate dynamics evolves on the flat portion of the boundary where the coupling conditions are implemented via the matching velocities of the plate and fluid flow, as well as the Dirichlet boundary trace of the pressure. This pressure term also acts as a coupling agent, since it appears as a forcing term on the flat, elastic plate domain. Our main focus in this work is to generate some numerical results concerning the approximate solutions to the FSI model. For this, we propose a numerical algorithm that sequentially solves the fluid and plate subsystems through an effective decoupling approach. Numerical results of test problems are presented to illustrate the performance of the proposed method.

KEYWORDS

biharmonic equation, Kirchhoff plate, Stokes fluid-plate interaction system

1 | INTRODUCTION

The qualitative and quantitative analysis of (PDE) systems, which are modeled via the interaction of a fluid flow with a deformable structure, have sparked great interest in the last decade. These fluid-structure interaction (FSI) dynamics appear in the modeling of a variety of physical phenomena, for example, the fluttering of an airplane/airfoil wing, the movement of wind turbines and bridges, blood transportation processes within arterial walls [3-5,8,9,11,15,21]. Since these systems are governed by multi-physics PDE models of generally high complexity, the theoretical and numerical analysis of solutions remain to be quite challenging.

Analytical results for various linear and nonlinear FSI PDE models, such as well-posedness and longtime behavior of solutions, have been studied in various settings; for example, [3-5,11,15]. The model of interest here, which describes the interaction of a 3D homogeneous viscous incompressible fluid with a 2D thin elastic plate, is well established in both physical and mathematical literature [2,12]. Moreover, these mathematical models are connected to FSI dynamics of the eye in biomedical applications. Basically, the ocular pressure in the eye plays a major role in the interaction process, and indeed the coupling in this model occurs through this pressure term [28]. In addition to eye dynamics, such FSI models describe the motions of a viscous incompressible fluid within a bounded cavity with elastic membrane. This is the problem of "sloshing" [22].

Our particular FSI describes the vibrations of the fluid within the 3D cavity as it interacts with the elastic membrane on the "free" upper boundary of the cavity. This model was initially considered in [12] from a theoretical point of view. In [12], the well-posedness result was initially shown via the Galerkin method. Subsequently, the authors analyzed the long time dynamics of the solutions in the sense of compact global attractors. In [2], the authors provided an alternative proof of well-posedness which relies on a semigroup formulation of the FSI model. In particular, their proof is based on generating a nonstandard mixed variational formulation and ultimately the application of the Babuska-Brezzi Theorem. We note that in [2], the obtained variational formulation is driven by the structure (plate) PDE component. However, in the current manuscript, we have a weak formulation given in Remark 3.2, which includes both the fluid and structure solution variables of the coupled PDE system. Also, the coupling of the parabolic and hyperbolic dynamics is given via both the matching velocity terms and the flux of the fluid (which is essentially the Dirichlet trace of the fluid pressure), as opposed to the matching fluxes of the fluid and plate dynamics. In turn, it is not all together clear how to decouple the given dynamics, and this is the heart of the matter in this manuscript.

Although the modeling and numerical analysis of "sloshing" PDE dynamics appears in the literature as a main application of 3D fluid-3D structure interactions [7], where a finite element method to approximate the vibration modes of a plate in contact with an incompressible fluid is analyzed, the body of work with respect to the quantitative properties and numerical analysis of such 3D-2D Stokes flow and plate interaction FSI systems is limited. This is in contrast to the present literature on the qualitative analysis of this particular FSI model. A very first numerical contribution to this model was made in [2], where the authors' well-posedness argument gives insight into a mixed finite element method (FEM) formulation in order to approximate the solution of the FSI system. In [2], some convergence results were provided for the approximation to the solutions, relative to "mesh parameter h," and moreover, an explicit numerical implementation of the derived mixed FEM was given. However, it should be noted that the authors in [2] operated in the frequency domain which requires solving the corresponding static PDE equations. As a result, the numerical method developed there solves and approximates static (time-independent) solution variables.

Our main goal in this manuscript is to develop an efficient numerical algorithm to approximate the solutions to the time-dependent FSI model using an accurate temporal discretization scheme. There

have been extensive studies on numerical methods for standard FSI problems with moving or non-moving interfaces, where the structure is modeled by linear [10,24] or nonlinear elasticity [5,6,25]. Numerical techniques for such problems are broadly classified as monolithic or partitioned methods. In a monolithic approach, the equations governing the fluid and structure, are integrated into a single unified system and solved simultaneously. This approach is known for its robust stability, making it advantageous in some applications. However, for the fluid-plate model where the plate structure is governed by the fourth-order PDE, a monolithic approach may not be desirable because the fluid and structure problems require different levels of solution regularity. The biharmonic operator within the plate equation presents a numerical challenge that arises from the necessity of utilizing finite elements of class C^1 for accurate approximation, while the fluid velocity can be simulated using C^0 class elements. Hence, we consider a domain decomposition approach for the coupled PDE system and develop a decoupling algorithm to solve the fluid and plate subproblems separately. The regularity issue associated with the biharmonic operator can be handled by either using mixed finite element methods [1,13,23], conforming high-order elements [34,36], or nonconforming elements such as Morley elements [27,30,31].

Our numerical algorithm is developed in the following way. Firstly, the model equations are discretized in time using a second-order temporal discretization scheme, and then a decoupling method is applied to the steady state problem at each time step. For the accuracy of the solution, we use an implicit approach, that is, the fluid and plate subsystems are solved sequentially until convergence is obtained. For the numerical analysis of the proposed method, we first show the stability of a solution to the continuous weak problem and then prove the stability of a solution to the semi-discrete (time-discretized) system. Numerical experiments are conducted for two examples. The first example is designed for the convergence test of the finite element solutions with a known exact solution, and the second examines the free vibration behavior of a plate. We choose using $P2-$Morley elements [16] for the plate subproblem in all the numerical simulations. Numerical findings regarding the 3D fluid-2D plate interaction system are relatively scarce in the literature. As mentioned before, only time-independent manufactured solutions are considered for the numerical experiment in [2]. *To the best of our knowledge*, this study marks the initial exploration of time discretization within the fluid-plate model system through numerical testing.

The paper is organized as follows. Section 2 introduces the model equations governing the interaction between a 3D fluid and a 2D plate structure. We present the weak formulation of the system and investigate its stability. In Section 4, we introduce and analyze the time discretization scheme for stability and present the computational algorithm for domain decomposition. Section 5 presents numerical results for test problems. Finally, the conclusion is provided in Section 6.

2 | MODEL EQUATIONS

We consider the structure domain $\Omega_p \subset \{x = (x_1, x_2, 0)\}$, and surface $S \subset \{x = (x_1, x_2, x_3) : x_3 \leq 0\}$ and the fluid domain $\Omega_f \subset \mathfrak{R}^3$ such that the boundary of Ω_f is $\partial\Omega_f := \overline{\Omega_p} \cup \overline{S}$. The domain Ω_f is occupied by the free fluid while the domain Ω_p indicates the plate region. See Figure 1. We consider the flow in Ω_f to be governed by the time-dependent Stokes equation and the plate structure is modeled by the "Euler–Bernoulli" or "Kirchhoff" equation. The fluid-plate system is then written as, for the final time $T > 0$:

$$\begin{cases} \mathbf{u}_t - \nu_f \Delta \mathbf{u} + \nabla p = \mathbf{f}_f & \text{in } \Omega_f \times (0, T), \\ \nabla \cdot \mathbf{u} = 0 & \text{in } \Omega_f \times (0, T), \\ \mathbf{u} = \mathbf{0} & \text{on } S \end{cases} \tag{2.1}$$

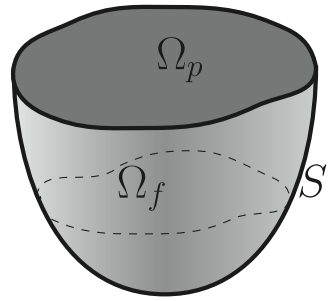

FIGURE 1 Fluid-structure interaction geometry.

$$\begin{cases} w_{tt} - \rho\Delta w_{tt} + \Delta^2 w = p|_{\Omega_p} & \text{in } \Omega_p \times (0,T), \\ w = \frac{\partial w}{\partial \mathbf{n}_p} = 0 & \text{on } \partial\Omega_p, \end{cases} \tag{2.2}$$

$$\mathbf{u} = [u_1, u_2, u_3] = [0, 0, w_t] \quad \text{on } \Omega_p \times (0,T), \tag{2.3}$$

where $\mathbf{u}(\mathbf{x},t)$ and $p(\mathbf{x},t)$ denote the fluid velocity and the fluid pressure respectively in Ω_f. And $\nu_f, \mathbf{f}_f(\mathbf{x},t)$ denote the constant fluid viscosity, and the body force, respectively. Furthermore, $w(\mathbf{x},t)$ is the displacement of the plate structure, and $\mathbf{n}_p$ denotes the outward unit normal vector to Ω_p. The constant $\rho \geq 0$ is the rotational inertia parameter which is proportional to the square of the thickness of the plate. The case $\rho = 0$ indicates that there is no rotational plate dynamics in play (i.e., the thickness of the plate is neglected), whereas $\rho > 0$ refers to the presence of rotational forces (full Kirchhoff plate). The model equations (2.1)-(2.3) are accompanied by the initial conditions

$$w = w_0, \ w_t = w_{t0}, \ \mathbf{u} = \mathbf{u}_0 \quad \text{at } t = 0.$$

3 | WEAK FORMULATION AND STABILITY ANALYSIS

We first derive a weak formulation of the problem using a Lagrange multiplier. We use the standard notation for Sobolev spaces and their associated norms and seminorms. We denote L^2 inner product and norm over Θ by $(\cdot,\cdot)_\Theta$ and $\|\cdot\|_\Theta$, respectively. Define

$$\begin{aligned} \mathbf{U} &:= \{\mathbf{v} = (v_1, v_2, v_3) \in \mathbf{H}^1(\Omega_f) : \ v_1 = v_2 = 0 \text{ on } \Omega_p, \mathbf{v} = \mathbf{0} \text{ on } S\}, \\ Q &:= L^2(\Omega_f), \\ W &:= \{z \in H^2(\Omega_p) : z = \frac{\partial z}{\partial \mathbf{n}_p} = 0 \text{ on } \partial\Omega_p\}. \end{aligned}$$

We also define the *div-free* space for the fluid velocity,

$$\mathbf{V} := \{\mathbf{v} \in \mathbf{U} : (q, \nabla \cdot \mathbf{v})_{\Omega_f} = 0, \forall q \in Q\},$$

and the mean zero space for the pressure,

$$Q_0 := L_0^2(\Omega_f) = \{q \in L^2(\Omega_f) : \int_{\Omega_f} q \, d\Omega_f = 0\}.$$

The spaces $\mathbf{U}$ and Q satisfy the inf-sup condition,

$$\inf_{q\in Q}\sup_{\mathbf{v}\in\mathbf{U}}\frac{(q,\nabla\cdot\mathbf{v})_{\Omega_f}}{\|q\|_{\Omega_f}\|\nabla\mathbf{v}\|_{\Omega_f}}\geq\beta>0. \tag{3.4}$$

The dual spaces $\mathbf{U}^*$ and $\mathbf{V}^*$ are endowed with the following dual norms

$$\|\mathbf{w}\|_{\mathbf{U}^*}:=\sup_{\mathbf{v}\in\mathbf{U}}\frac{(\mathbf{w},\mathbf{v})_{\Omega_f}}{\|\nabla\mathbf{v}\|_{\Omega_f}},\quad \|\mathbf{w}\|_{\mathbf{V}^*}:=\sup_{v\in\mathbf{V}}\frac{(\mathbf{w},\mathbf{v})_{\Omega_f}}{\|\nabla\mathbf{v}\|_{\Omega_f}}.$$

These norms are equivalent for functions in $\mathbf{V}$. See Lemma 1 in [17]. For the variational formulation of (2.1) and (2.2) with the constraint (2.3), we introduce a Lagrange multiplier $g\in G:=H^{-1/2}(\Omega_p)$, representing

$$g:=(\boldsymbol{\sigma}_f\mathbf{n}_f)_3\quad\text{on }\Omega_p\times(0,T), \tag{3.5}$$

where $\boldsymbol{\sigma}_f=\nu_f\nabla\mathbf{u}-p\mathbf{I}$ and $\mathbf{n}_f=[0\ 0\ 1]^T$. Given the Babuska–Brezzi problem in Remark 3.2 is well-posed, we note that the normal component of the Stokes flux $(\boldsymbol{\sigma}_f\mathbf{n}_f)$ is well defined on the boundary portion Ω_p, and $g:=(\boldsymbol{\sigma}_f\mathbf{n}_f)_3\in H^{-1/2}(\Omega_p)$ (See [35, page 9, Theorem 1.2]).

Remark 3.1. When the plate model (2.2) was introduced in [12], the original equation included the surface forcing term $(-\boldsymbol{\sigma}_f\mathbf{n}_f)|_{\Omega_p}$ exerted by the fluid on the plate. Since $\mathbf{n}_f=[0\ 0\ 1]^T$, the stress force is simplified to $\nu_f\partial_z u_3-p$, and the *div free* condition $\nabla\cdot\mathbf{u}=0$ in Ω_f together with the boundary condition $(u_1,u_2)=(0,0)$ on Ω_p yield $\partial_z u_3=0$ on Ω_p. See [12] for details. Hence, the pressure function in (2.2) is indeed identical to $-(\boldsymbol{\sigma}_f\mathbf{n}_f)_3$ in Ω_p and can be represented by the Lagrange multiplier function $-g$.

In the weak formulation followed, the Lagrange multiplier function g will replace the pressure in the plate equation. We now multiply the governing equations by appropriate test functions and use integration by parts to obtain the following continuous variational formulation:

Given the initial conditions, find $(\mathbf{u},p,w,g)\in(\mathbf{U},Q,W,G)$, *for a.e.* $t\in(0,T)$, *such that*

$$(\mathbf{u}_t,\ \mathbf{v})_{\Omega_f}+(\nu_f\nabla\mathbf{u},\nabla\mathbf{v})_{\Omega_f}-(p,\nabla\cdot\mathbf{v})_{\Omega_f}-(g,v_3)_{\Omega_p}=(\mathbf{f}_f,\mathbf{v})_{\Omega_f}\quad\forall\mathbf{v}\in\mathbf{U}, \tag{3.6}$$

$$(q,\nabla\cdot\mathbf{u})_{\Omega_f}=0,\quad\forall q\in Q, \tag{3.7}$$

$$(w_{tt},\ z)_{\Omega_p}+\rho(\nabla w_{tt},\nabla z)_{\Omega_p}+(\Delta w,\Delta z)_{\Omega_p}+(g,z)_{\Omega_p}=0\quad\forall z\in W, \tag{3.8}$$

$$(w_t-u_3,\lambda)_{\Omega_p}=0,\quad\forall\lambda\in G. \tag{3.9}$$

Note that (3.9) weakly enforces continuity of velocity at the plate structure.

Remark 3.2. If we define the bilinear form $B(\cdot,\cdot):(\mathbf{U}\times W)\times(Q\times G)\to\mathfrak{R}$ by

$$B((\mathbf{v},z),(q,h)):=-(q,\nabla\cdot\mathbf{v})_{\Omega_f}-(v_3-z,h)_{\Omega_p},$$

the system (3.6)-(3.9) has the structure of a saddle point problem

$$A((\mathbf{u},w),(\mathbf{v},z))+B((\mathbf{v},z),(p,g))=(\mathbf{f}_f,\mathbf{v})_{\Omega_f},$$
$$B((\mathbf{u},w_t),(q,\lambda))=0,$$

where

$$A((\mathbf{u},w),(\mathbf{v},z)):=(\mathbf{u}_t,\ \mathbf{v})_{\Omega_f}+(\nu_f\nabla\mathbf{u},\nabla\mathbf{v})_{\Omega_f}+(w_{tt},\ z)_{\Omega_p}+\rho(\nabla w_{tt},\nabla z)_{\Omega_p}+(\Delta w,\Delta z)_{\Omega_p}.$$

The inf-sup condition of $B(\cdot,\cdot)$ has been proved in [14] for the time-discretized Stokes-linear elasticity FSI system, where the structure equation is the 2nd order PDE and the displacement has an H^1-regularity. We believe a similar approach can be used for the inf-sup condition of $B(\cdot,\cdot)$ with the H^2-regular displacement. Also, when time-discretized, the associated bilinear form $A(\cdot,\cdot)$ can be shown to be coercive and continuous in the corresponding function spaces. Since this work focuses on the study of the numerical algorithms for time-stepping, stability analysis, and implementation of a partitioning method, the well-posedness is not considered here but will be investigated in a later work.

To study the stability of the semi-discrete system in the following section, in the next theorem, we establish the stability of a weak solution to the system (3.6)–(3.9). Since the unknown forcing term g represents the pressure on Ω_p in the current problem setting with $\mathbf{n} = [0\,0\,1]^T$, we will keep utilizing the general force g as formulated in (3.8) instead of $-p$ and show the pressure stability in terms of the given data and the forcing function g.

Theorem 3.3. *For any $\mathbf{f}_f \in L^2(0,T,\mathbf{L}^2(\Omega_f))$ a solution to (3.6)–(3.9) is stable. For any $t > 0$ and $C_{PF} > 0$,*

$$\|\mathbf{u}\|^2_{\Omega_f} + \nu_f \int_0^t \|\nabla \mathbf{u}\|^2_{\Omega_f} ds + \|w_t\|^2_{\Omega_p} + \rho\|\nabla w_t\|^2_{\Omega_p} + \|\Delta w\|^2_{\Omega_p} \le \frac{C_{PF}}{\nu_f}\int_0^t \|\mathbf{f}_f\|^2_{\Omega_f} ds + C_0, \tag{3.10}$$

where $C_0 = \|\mathbf{u}_0\|^2_{\Omega_f} + \|w_{t0}\|^2_{\Omega_p} + \rho\|\nabla w_{t0}\|^2_{\Omega_p} + \|\Delta w_0\|^2_{\Omega_p}$. Furthermore, for some $C_\beta > 0$, we have

$$\int_0^t \|p\|^2_{\Omega_f} ds \le C_\beta\left(\int_0^t \|\mathbf{f}_f\|^2_{\Omega_f} ds + \int_0^t \|g\|^2_{H^{-1/2}(\Omega_p)} ds + C_0\right). \tag{3.11}$$

Proof. Choose $\mathbf{v} = \mathbf{u}$ in (3.6), $q = p$ in (3.7), $z = w_t$ in (3.8) and $\lambda = g$ in (3.9). Adding all the terms together, we get

$$(\mathbf{u}_t,\ \mathbf{u}) + \nu_f\|\nabla \mathbf{u}\|^2_{\Omega_f} + (w_{tt}, w_t)_{\Omega_p} + \rho(\nabla w_{tt}, \nabla w_t)_{\Omega_p} + (\Delta w, \Delta w_t)_{\Omega_p} = (\mathbf{f}_f, \mathbf{u})_{\Omega_f},$$

and, using Cauchy–Schwarz inequality, and multiplying by 2 on both sides, we get

$$\frac{d}{dt}\|\mathbf{u}\|^2_{\Omega_f} + 2\nu_f\|\nabla \mathbf{u}\|^2_{\Omega_f} + \frac{d}{dt}\|w_t\|^2_{\Omega_p} + \rho\frac{d}{dt}\|\nabla w_t\|^2_{\Omega_p} + \frac{d}{dt}\|\Delta w\|^2_{\Omega_p} \le 2\|\mathbf{f}_f\|_{\Omega_f}\|\mathbf{u}\|_{\Omega_f}.$$

Integrate over (0,t) for a.e. $t \in (0,T)$ to obtain

$$\begin{aligned}&\|\mathbf{u}\|^2_{\Omega_f} + 2\nu_f\int_0^t \|\nabla \mathbf{u}\|^2_{\Omega_f} ds + \|w_t\|^2_{\Omega_p} + \rho\|\nabla w_t\|^2_{\Omega_p} + \|\Delta w\|^2_{\Omega_p}\\ &\le 2\int_0^t \|\mathbf{f}_f\|_{\Omega_f}\|\mathbf{u}\|_{\Omega_f}\, ds + \|\mathbf{u}_0\|^2_{\Omega_f} + \|w_{t0}\|^2_{\Omega_p} + \rho\|\nabla w_{t0}\|^2_{\Omega_p} + \|\Delta w_0\|^2_{\Omega_p}.\end{aligned} \tag{3.12}$$

Then, Young's inequality and Poincare Friedrich's inequality yield, for some $\epsilon > 0$ and $C_{PF} > 0$,

$$\int_0^t \|\mathbf{f}_f\|_{\Omega_f}\|\mathbf{u}\|_{\Omega_f}\, ds \le \frac{1}{2\epsilon}\int_0^t \|\mathbf{f}_f\|^2_{\Omega_f} ds + \frac{\epsilon C_{PF}}{2}\int_0^t \|\nabla \mathbf{u}\|^2_{\Omega_f} ds.$$

Using this estimate and setting $\epsilon = (\nu_f/C_{PF})$ in (3.12), we obtain (3.10).

To estimate the bound for the pressure p, we use a similar approach mentioned in [20]. We first estimate a bound for the time derivative of the flow velocity term in (3.6). For $\mathbf{v} \in \mathbf{V}$ the equation (3.6) is written as

$$(\mathbf{u}_t, \mathbf{v})_{\Omega_f} = -\nu_f(\nabla \mathbf{u}, \nabla \mathbf{v})_{\Omega_f} + (\mathbf{f}_f, \mathbf{v})_{\Omega_f} + (g, v_3)_{\Omega_p}. \tag{3.13}$$

The last term on the right-hand side of (3.13) is bounded as

$$(g, v_3)_{\Omega_p} \leq \|g\|_{H^{-1/2}(\Omega_p)} \|\mathbf{v}\|_{H^{1/2}(\Omega_p)} \leq C \|g\|_{H^{-1/2}(\Omega_p)} \|\mathbf{v}\|_{H^1(\Omega_f)},$$

using the trace theorem. Now, using Cauchy–Schwarz inequality and Poincaré–Friedrichs inequality in (3.13), we have, for some constant $\widehat{C} > 0$,

$$\|\mathbf{u}_t\|_{\mathbf{V}^*} \leq \widehat{C}(\|\nabla \mathbf{u}\|_{\Omega_f} + \|\mathbf{f}_f\|_{\Omega_f} + \|g\|_{H^{-1/2}(\Omega_p)}).$$

The norm equivalence of $\|\cdot\|_{\mathbf{U}^*}$ and $\|\cdot\|_{\mathbf{V}^*}$ (see Lemma 1 in [17]) then implies, for some constant $C_* > 0$,

$$\|\mathbf{u}_t\|_{\mathbf{U}^*} \leq C_*(\|\nabla \mathbf{u}\|_{\Omega_f} + \|\mathbf{f}_f\|_{\Omega_f} + \|g\|_{H^{-1/2}(\Omega_p)}). \tag{3.14}$$

To estimate a bound for the pressure term p, consider (3.6) with $\mathbf{v} \in \mathbf{U}$. We isolate the pressure term, divide by $\|\nabla \mathbf{v}\|_{\Omega_f}$, take supremum over $\mathbf{v} \in \mathbf{U}$. Then the inf-sup condition (3.4) and the estimate (3.14) yield

$$\beta \|p\|_{\Omega_f} \leq (1 + C_*)(\|\nabla \mathbf{u}\|_{\Omega_f} + \|\mathbf{f}_f\|_{\Omega_f} + \|g\|_{H^{-1/2}(\Omega_p)}).$$

for some $\beta > 0$. Finally, we square both sides, integrate over $(0, t)$, use (3.10), to obtain

$$\int_0^t \|p\|^2_{\Omega_f} ds \leq C_\beta \left(\int_0^t \|\mathbf{f}_f\|^2_{\Omega_f} ds + \int_0^t \|g\|^2_{H^{-1/2}(\Omega_p)} ds + C_0 \right)$$

or some constant $C_\beta > 0$. ∎

4 | TEMPORAL DISCRETIZATION SCHEME

In this section, we discuss the second-order temporal discretization scheme for the fluid-plate system and study its stability. To discretize the above equations in time, we set for $T > 0$, $\tau = T/M$, where M is a positive integer and we set for $n = 0, 1, 2, \ldots, M$, $t_n = n\tau$. For any sufficiently smooth function $v(\mathbf{x}, t)$, both constant and vector-valued, we define $v^n(\mathbf{x}) \sim v(\mathbf{x}, t_n)$. The fluid equations are discretized in time using a second-order Crank–Nicolson scheme while the plate equations are discretized using a second-order Newmark scheme [26]. Further, we introduce an additional variable $\dot{w} \in W$, representing w_t in the plate subsystem. Also, denote for any function ϕ,

$$\overline{\phi}^n = \frac{\phi^n + \phi^{n-1}}{2}.$$

Consider the semi-discrete fluid-plate system:

$$\rho_f(\mathbf{u}^n - \mathbf{u}^{n-1}) - \nu_f \tau \Delta \overline{\mathbf{u}}^n + \tau \nabla \overline{p}^n = \tau \overline{\mathbf{f}}_f^n \quad \text{in } \Omega_f, \tag{4.15}$$

$$\nabla \cdot \overline{\mathbf{u}}_n = 0 \quad \text{in } \Omega_f, \tag{4.16}$$

$$(\dot{w}^n - \dot{w}^{n-1}) - \rho \Delta (\dot{w}^n - \dot{w}^{n-1}) + \tau \Delta^2 \overline{w}^n = \tau \overline{p}^n|_{\Omega_p} \quad \text{in } \Omega_p, \tag{4.17}$$

$$w^n - w^{n-1} = \tau \overline{\dot{w}}^n \quad \text{in } \Omega_p, \tag{4.18}$$

$$\overline{u_3}^n = \overline{\dot{w}}^n \quad \text{in } \Omega_p. \tag{4.19}$$

In the next theorem, we show the stability of the numerical scheme.

Theorem 4.1. *The method (4.15)–(4.19) is unconditionally stable. Moreover, for some constants $C_M, C_T > 0$, and for any t_n, the following relations hold*:

$$\rho_f\|\mathbf{u}^M\|^2_{\Omega_f} + 2\nu_f\tau\sum_{n=0}^{M}\|\nabla\overline{\mathbf{u}}^n\|^2_{\Omega_f} + \|\dot{w}^M\|^2_{\Omega_p} + \|\Delta w^M\|^2_{\Omega_p} + \rho\|\nabla\dot{w}^M\|^2_{\Omega_p} \le \frac{\tau C_M}{\nu_f}\sum_{n=0}^{M}\|\overline{\mathbf{f}}_f^n\|^2_{\Omega_f}, \tag{4.20}$$

$$\|w^n\|^2_{\Omega_p} \le \frac{(C_T\tau)^2 C_M}{4\nu_f}\sum_{n=0}^{M}\|\overline{\mathbf{f}}_f^n\|^2_{\Omega_f}. \tag{4.21}$$

Additionally, we have

$$\|\overline{p}^n\|^2_{\Omega_f} \le C_\beta(\ \|\overline{\mathbf{f}}_f^n\|^2_{\Omega_f} + \|\overline{g}^n\|^2_{H^{-1/2}(\Omega_p)}\ ) \tag{4.22}$$

for some $C_\beta > 0$.

Proof. For simplicity, let $\mathbf{u}_0 = \mathbf{0}$ and $w_0 = w_{t0} = 0$. Multiplying (4.15) and (4.16) by $\overline{\mathbf{u}}^n$ and $\overline{p}^n$ respectively, integrating over Ω_p, and adding the results yield

$$\frac{\rho_f}{2}\left(\|\mathbf{u}^n\|^2_{\Omega_f} - \|\mathbf{u}^{n-1}\|^2_{\Omega_f}\right) + \nu_f\tau\|\nabla\overline{\mathbf{u}}^n\|^2_{\Omega_f} \le \tau(\overline{\mathbf{f}}_f^n, \overline{\mathbf{u}}^n)_{\Omega_f} + \tau(\overline{g}^n, \overline{u_3^n})_{\Omega_p}. \tag{4.23}$$

Similarly, multiplying (4.17) by $\overline{\dot{w}}^n$ and integrating over Ω_p give:

$$(\dot{w}^n - \dot{w}^{n-1}, \overline{\dot{w}}^n)_{\Omega_p} - (\rho\Delta(\dot{w}^n - \dot{w}^{n-1}), \overline{\dot{w}}^n)_{\Omega_p} + (\Delta^2\overline{w}^n, \tau\overline{\dot{w}}^n)_{\Omega_p} = \tau(\overline{p}^n, \overline{\dot{w}}^n)_{\Omega_p}. \tag{4.24}$$

Note that, using Green's theorem,

$$(\Delta^2\overline{w}^n, \tau\overline{\dot{w}}^n)_{\Omega_p} = -(\nabla\Delta\overline{w}^n, \nabla\tau\overline{\dot{w}}^n)_{\Omega_p} = (\Delta\overline{w}^n, \Delta\tau\overline{\dot{w}}^n)_{\Omega_p} \tag{4.25}$$

and

$$-(\rho\Delta(\dot{w}^n - \dot{w}^{n-1}), \overline{\dot{w}}^n)_{\Omega_p} = (\rho\nabla(\dot{w}^n - \dot{w}^{n-1}), \nabla\overline{\dot{w}}^n)_{\Omega_p}, \tag{4.26}$$

since $\overline{\dot{w}}^n$ and $\frac{\partial\overline{\dot{w}}^n}{\partial\mathbf{n}_p}$ are zero on $\partial\Omega_p$ by (4.18). Then, (4.18) and (4.24)–(4.26) yield

$$(\dot{w}^n - \dot{w}^{n-1}, \overline{\dot{w}}^n)_{\Omega_p} + (\rho\nabla(\dot{w}^n - \dot{w}^{n-1}), \nabla\overline{\dot{w}}^n)_{\Omega_p} + (\Delta\overline{w}^n, \Delta(w^n - w^{n-1}))_{\Omega_p} = \tau(\overline{p}^n, \overline{\dot{w}}^n)_{\Omega_p}. \tag{4.27}$$

This implies

$$\frac{1}{2}\left(\|\dot{w}^n\|^2_{\Omega_p} - \|\dot{w}^{n-1}\|^2_{\Omega_p}\right) + \frac{\rho}{2}\left(\|\nabla\dot{w}^n\|^2_{\Omega_p} - \|\nabla\dot{w}^{n-1}\|^2_{\Omega_p}\right) + \frac{1}{2}\left(\|\Delta w^n\|^2_{\Omega_p} - \|\Delta w^{n-1}\|^2_{\Omega_p}\right) = \tau(\overline{p}^n, \overline{\dot{w}}^n) \tag{4.28}$$

Also, multiplying (4.19) by $\overline{g}^n$ and integrating over Ω_p, we have

$$(\overline{u_3^n}, \overline{g}^n)_{\Omega_p} = (\overline{\dot{w}}^n, \overline{g}^n)_{\Omega_p}. \tag{4.29}$$

Using (4.29) with $\overline{g}^n = -\overline{p}^n$ in (4.23) (see Remark 3.1) and adding (4.23) to (4.28), we obtain

$$\begin{aligned}&\frac{\rho_f}{2}\left(\|\mathbf{u}^n\|^2_{\Omega_f} - \|\mathbf{u}^{n-1}\|^2_{\Omega_f}\right) + \nu_f\tau\|\nabla\overline{\mathbf{u}}^n\|^2_{\Omega_f} + \frac{1}{2}\left(\|\dot{w}^n\|^2_{\Omega_p} - \|\dot{w}^{n-1}\|^2_{\Omega_p}\right)\\ &\quad + \frac{1}{2}\left(\|\Delta w^n\|^2_{\Omega_p} - \|\Delta w^{n-1}\|^2_{\Omega_p}\right) + \frac{\rho}{2}\left(\|\nabla\dot{w}^n\|^2_{\Omega_p} - \|\nabla\dot{w}^{n-1}\|^2_{\Omega_p}\right)\\ &\le \tau(\overline{\mathbf{f}}_f^n, \overline{\mathbf{u}}^n)_{\Omega_f}\ \le \tau\|\overline{\mathbf{f}}_f^n\|_{\Omega_f}\|\overline{\mathbf{u}}^n\|_{\Omega_f}.\end{aligned}$$

Now, Young's inequality and Poincare–Friedrich's inequality for any $\epsilon > 0$ and for some $C_{PF} > 0$ give

$$\frac{\rho_f}{2}\left(\|\mathbf{u}^n\|^2_{\Omega_f} - \|\mathbf{u}^{n-1}\|^2_{\Omega_f}\right) + \nu_f\tau\|\nabla\overline{\mathbf{u}}^n\|^2_{\Omega_f} + \frac{1}{2}\left(\|\dot{w}^n\|^2_{\Omega_p} - \|\dot{w}^{n-1}\|^2_{\Omega_p}\right) + \frac{1}{2}\left(\|\Delta w^n\|^2_{\Omega_p} - \|\Delta w^{n-1}\|^2_{\Omega_p}\right) + \frac{\rho}{2}\left(\|\nabla\dot{w}^n\|^2_{\Omega_p} - \|\nabla\dot{w}^{n-1}\|^2_{\Omega_p}\right) \leq \frac{\tau}{2\epsilon}\|\overline{\mathbf{f}}^n_f\|^2_{\Omega_f} + \frac{\epsilon C_{PF}\tau}{2}\|\nabla\overline{\mathbf{u}}^n\|^2_{\Omega_f}.$$

Setting $\epsilon = \nu_f/(C_{PF})$ and summing from $n = 0$ to M, we get, for some constant $C_M > 0$

$$\rho_f\|\mathbf{u}^M\|^2_{\Omega_f} + \nu_f\tau\sum_{n=0}^{M}\|\nabla\overline{\mathbf{u}}^n\|^2_{\Omega_f} + \|\dot{w}^M\|^2_{\Omega_p} + \|\Delta w^M\|^2_{\Omega_p} + \rho\|\nabla\dot{w}^M\|^2_{\Omega_p} \leq \frac{\tau C_M}{2\nu_f}\sum_{n=0}^{M}\|\overline{\mathbf{f}}^n_f\|^2_{\Omega_f}. \quad (4.30)$$

We multiply (4.19) by $\overline{\dot{w}}^n$, integrate over Ω_p, and use Cauchy–Schwarz inequality to obtain,

$$\|\overline{\dot{w}}^n\|^2_{\Omega_p} \leq \|\overline{u_3^n}\|_{\Omega_p}\|\overline{\dot{w}}^n\|_{\Omega_p}.$$

Applying the trace theorem and Young's inequality, for some $C_T > 0$,

$$\|\overline{\dot{w}}^n\|^2_{\Omega_p} \leq C_T\|\nabla\overline{\mathbf{u}}^n\|_{\Omega_f}\|\overline{\dot{w}}^n\|_{\Omega_p} \leq \frac{C_T^2}{2}\|\nabla\overline{\mathbf{u}}^n\|^2_{\Omega_f} + \frac{1}{2}\|\overline{\dot{w}}^n\|^2_{\Omega_p},$$

which implies

$$\|\overline{\dot{w}}^n\|^2_{\Omega_p} \leq C_T^2\|\nabla\overline{\mathbf{u}}^n\|^2_{\Omega_f}.$$

Next, multiply (4.18) with $w^n - w^{n-1}$, integrate over Ω_p and use Cauchy–Schwarz inequality.

$$\begin{aligned} &\|w^n - w^{n-1}\|^2_{\Omega_p} \leq \tau\|\overline{\dot{w}}^n\|_{\Omega_p}\|w^n - w^{n-1}\|_{\Omega_p}, \\ \Rightarrow\ &\frac{1}{2}\|w^n - w^{n-1}\|^2_{\Omega_p} \leq \frac{\tau^2}{2}\|\overline{\dot{w}}^n\|^2_{\Omega_p}, \\ \Rightarrow\ &\frac{1}{2}\|w^n\|^2_{\Omega_p} - \frac{1}{2}\|w^{n-1}\|^2_{\Omega_p} \leq \frac{\tau^2}{2}\|\overline{\dot{w}}^n\|^2_{\Omega_p}. \end{aligned} \quad (4.32)$$

Finally using (4.31) in (4.32), summing from $n = 0$ to $n = m$, where $m \in \{1, 2, \dots, M\}$, we get

$$\|w^n\|^2_{\Omega_p} \leq (C_T\tau)^2\sum_{n=0}^{m}\|\nabla\overline{\mathbf{u}}^n\|^2_{\Omega_f} \leq (C_T\tau)^2\sum_{n=0}^{M}\|\nabla\overline{\mathbf{u}}^n\|^2_{\Omega_f}. \quad (4.33)$$

For the stability of p^n, we mimic the proof of the continuous case. We isolate the pressure term in (4.15), multiply with $\mathbf{u}^n$, integrate over Ω_f and divide by $\|\nabla\mathbf{v}\|_{\Omega_f}$ and take supremum over $\mathbf{v} \in \mathbf{U}$. Then, the inf-sup condition (3.4) yields that

$$\beta\|\overline{p}^n\|_{\Omega_f} \leq (1 + C_*)(\ \|\nabla\overline{\mathbf{u}}^n\|_{\Omega_f} + \|\overline{\mathbf{f}}^n_f\|_{\Omega_f} + \|\overline{g}^n\|_{H^{-1/2}(\Omega_p)}) \quad (4.34)$$

for some $\beta, C_* > 0$. Squaring on both sides of (4.34), using $(a + b + c)^2 \leq 3(a^2 + b^2 + c^2)$ on the right side and finally using (4.30), we get, for some $C_\beta > 0$,

$$\|\overline{p}^n\|^2_{\Omega_f} \leq C_\beta(\ \|\overline{\mathbf{f}}^n_f\|^2_{\Omega_f} + \|\overline{g}^n\|^2_{H^{-1/2}(\Omega_p)}\ ). \quad (4.35)$$

(4.35) now implies the stability of p^n. ∎

For the numerical simulation of the coupled fluid-plate system, we employ a partitioning method using fixed-point iteration. In this approach, we impose the condition $u_3 = w_t$ strongly as the

Dirichlet condition for the fluid problem. Each time step begins with solving the fluid subproblem, where an initial guess for $\dot{w}$ is used, followed by solving the plate equation using the pressure. The fluid and the plate subsystem are solved serially and implicitly in time using iterations that terminate when the relative residual is smaller than a chosen tolerance. However, an issue arises when solving the subsystems separately using Dirichlet conditions. Because the pressure is not uniquely determined, an appropriate shifting method needs to be developed. Note that $\int_{\Omega_p} w_t \, d\Omega_p = \int_{\Omega_p} u_3 \, d\Omega_p = \int_{\partial\Omega_f} \mathbf{u} \cdot \mathbf{n}_f \, d(\partial\Omega_f) = 0$ due to the incompressibility condition $\nabla \cdot \mathbf{u} = 0$ [2,18]. This additional constraint can be incorporated into the plate system to determine the correct pressure. At the k-th fixed point iteration, the pressure, $\hat{p}$ is computed with the mean zero condition. Subsequently, the plate problem is solved for the additional unknown scalar value s with the pressure p replaced by $\hat{p} - s$ in (4.17) and the additional constraint equation $\int_{\Omega_p} \dot{w} \, d\Omega_p = 0$. Then $\hat{p} - s$ is expected to be the pressure satisfying (4.15)–(4.19) [33]. We summarize the complete numerical algorithm in Algorithm 1.

Algorithm 1. Working algorithm

Input: $\dot{w}$ initial guess, ϵ tolerance and N_{iter} maximum number of iteration.
Output: $\dot{w}^{n,k}$
$k = 0$, error $>\epsilon$, $\dot{w}^{0,0} = 0, \mathbf{u}^{0,0} = \mathbf{0}$
for $n = 1, 2, 3, \dots, N$
while $k<N_{\text{iter}}$ and error $>\epsilon$, **do**

1. Solve for $(\mathbf{u}^{n,k}, \hat{p}^{n,k}) \in \mathbf{U} \times Q_0$ with $u_3^{n,k} = \dot{w}^{n,k-1}$:

$$\begin{aligned} \mathbf{u}^{n,k} - \nu_f \tau \Delta \overline{\mathbf{u}}^{n,k} + \tau \nabla \overline{\hat{p}}^{n,k} &= \tau \overline{\mathbf{f}}_f^{n,k} - \mathbf{u}^{n-1,k} \quad \text{in } \Omega_f, \\ \nabla \cdot \overline{\mathbf{u}}^{n,k} &= 0 \quad \text{in } \Omega_f, \\ \mathbf{u}^{n,k} &= \mathbf{0} \quad \text{on } S, \\ \mathbf{u}^{n,k} = [u_1^{n,k}, u_2^{n,k}, u_3^{n,k}] &= [0, 0, \dot{w}^{n,k-1}] \quad \text{on } \Omega_p, \\ \int_{\Omega_f} \hat{p}^{n,k} \, d\Omega_f &= 0. \end{aligned} \tag{36}$$

2. Solve for $(w^{n,k}, \dot{w}^{n,k}, s^{n,k})$ in $W \times W \times R$:

$$\begin{aligned} \dot{w}^{n,k} - \rho \Delta \dot{w}^{n,k} + \tau \Delta^2 \overline{w}^{n,k} &= \tau \left(\overline{\hat{p}}^{n,k}|_{\Omega_p} - s^{n,k} \right) + \dot{w}^{n-1,k} - \rho \Delta \dot{w}^{n-1,k} \quad \text{in } \Omega_p, \\ w^{n,k} - w^{n-1,k} &= \tau \overline{\dot{w}}^{n,k} \quad \text{in } \Omega_p, \\ \int_{\Omega_p} \dot{w}^{n,k} \, d\Omega_f &= 0, \\ w^{n,k} = \frac{\partial w^{n,k}}{\partial \nu} &= 0 \quad \text{on } \partial\Omega_p. \end{aligned} \tag{37}$$

3. Update $\dot{w}^{n,k-1} = \dot{w}^{n,k}$.

end while
Set $p^n = \hat{p}^{n,k} - s^{n,k}$
Reset $k = 0$.
end for

5 | NUMERICAL RESULTS

5.1 | Test 1: Manufactured solutions

In this section, we introduce manufactured solutions for the fluid-plate system and illustrate the behavior of the method by performing convergence tests. All computations are performed using freefem++ [19]. We consider the domains $\Omega_f = [0,1]\times[0,1]\times[-1,0]$ and $\Omega_p = [0,1]\times[0,1]\times\{0\}$. See Figure 2 for the computational domain. Further, the manufactured fluid velocity, pressure and plate displacement are considered as follows:

$$\begin{aligned}
u_1 &= (2x^3(x-1)^3(9x^2-9x+2)y^4(y-1)^4,\\
&\quad + (4/5)x^5(x-1)^5y^2(y-1)^2(14y^2-14y+3))(-30z^4-60z^3-30z^2)e^{-t},\\
u_2 &= 0,\\
u_3 &= x^4(x-1)^4(2x-1)y^4(y-1)^4(-6z^5-15z^4-10z^3-1)e^{-t},\\
p &= 0,\\
w &= x^4(x-1)^4(2x-1)y^4(y-1)^4e^{-t}.
\end{aligned}$$

Note that at $z = 0, u_3 = w_t$. The right-hand side function $\mathbf{f}_f$ is computed using the manufactured solution. For the finite elements simulation, we used $(\mathbf{P}_2, P_1, P_2\text{Morley}, P_2)$ elements for $(\mathbf{u}, p, w, w_t)$. We set final time $T_{\text{final}} = 0.01$ and $\tau = 0.001$ and evaluated errors and convergence rates for different values of N (see Tables 1 and 2). We observed that the H^1- and H^2- rates of the structure are well matched with the theoretical convergence rates [29], while L^2 rates are not optimal for smaller h with the chosen time step $\tau = 0.001$. Furthermore, we plot and compare the finite element solution, w_t-FEM and u_3-FEM, with exact solutions, w_t-Exact and u_3-Exact, in Figures 3 and 4. The observation that both w_t and u_3 functions exhibit identical behavior in the plotted solutions indicates a strong agreement between the numerical model and the theoretical expectations.

While performing convergence tests in time, Freefem++ did not allow us to set spatial mesh size smaller than $\frac{1}{13}$ as the problem becomes very large due to the involvement of 3D fluid equations. On using spatial mesh size $\frac{1}{12}$, we obtained that the errors evaluated for different time steps are very small; however, they are flat (see Table 3). We then solved only the 2D plate equation in the domain $[0,1]\times[0,1]$ using the exact solution and first-order time discretization and observed similar flat errors. To address this issue, we used a very large weight (10^5) in the w_{tt} term of the structure equation for spatial mesh size $\frac{1}{50}$, which allowed us to achieve linear convergence in time (see Table 4). With the weight, the structure problem is defined as follows:

$$(\text{weight})w_{tt} - \rho\Delta w_{tt} + \Delta^2 w = f_p,$$

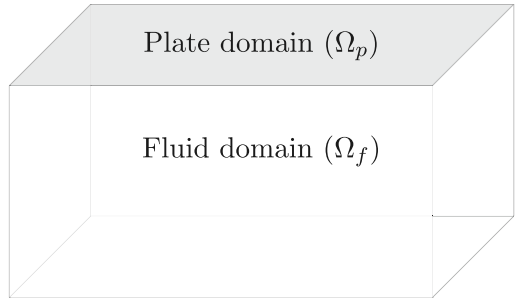

FIGURE 2 3D Fluid and 2D plate system for numerical tests.

TABLE 1 Errors and convergence rates for **u** and p functions at final time $T_{\text{final}} = 0.01$ using time-step size $\Delta t = 0.001$ for different values of h.

h	L^2(Velocity)	H^1(Velocity)	L^2(pressure)
1/4	$1.77e-06$	$4.70e-05$	$6.58e-06$
1/6	$4.78e-04$[3.23]	$2.19e-05$[1.88]	$2.82e-06$[2.09]
1/8	$2.02e-07$[2.99]	$1.30e-05$[1.81]	$1.12e-06$[3.20]
1/10	$1.09e-07$[2.75]	$8.78e-06$[1.76]	$5.05e-07$[3.59]
1/12	$6.68e-08$[2.73]	$6.34e-06$[1.79]	$2.72e-07$[3.39]

TABLE 2 Errors and convergence rates for w function at final time $T_{\text{final}} = 0.01$ using time-step size $\Delta t = 0.001$ for different values of h.

h	L^2(w-function)	H^1(w-function)	H^2(w-function)
1/4	$2.22e-07$	$3.13e-06$	$5.83e-05$
1/6	$8.49e-08$[2.37]	$1.40e-06$[1.99]	$4.25e-05$[0.78]
1/8	$3.28e-08$[3.31]	$7.33e-07$[2.24]	$3.15e-05$[1.04]
1/10	$2.06e-08$[2.09]	$4.87e-07$[1.83]	$2.59e-05$[0.88]
1/12	$1.48e-08$[1.80]	$3.17e-07$[2.36]	$2.10e-05$[1.16]]

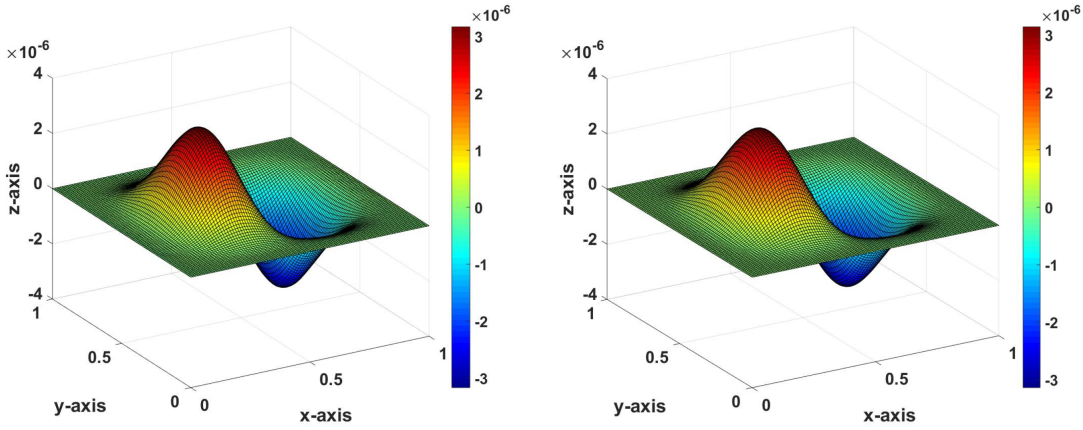

FIGURE 3 w_t-FEM (left) and w_t-Exact (right) for $h = 1/12$, $T_{\text{final}} = 0.01$, $\tau = 0.001$.

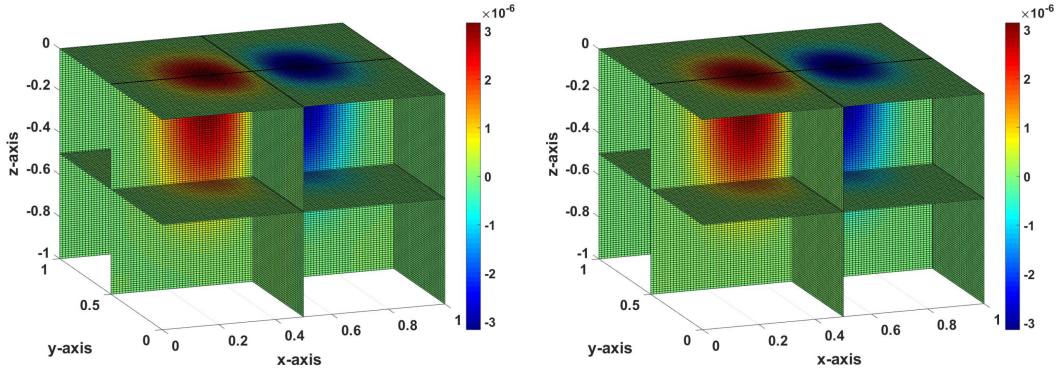

FIGURE 4 u_3-FEM (left) and u_3-Exact (right) for $h = 1/12$, $T_{\text{final}} = 0.01$, $\tau = 0.001$.

TABLE 3 Flat errors for w function at final time $T_{\text{final}} = 0.2$ using mesh size $\frac{1}{12}$ using $\Delta t = \{0.2, 0.1, 0.05, 0.025\}$.

Type	Error
L^2(w-function)	$1.90e-07$
H^1(w-function)	$1.65e-06$
H^2(w-function)	$2.45e-05$

TABLE 4 L^2 errors and convergence rates for w function at final time $T_{\text{final}} = 4$ using the first-order time discretization method with mesh size $\frac{1}{50}$ while solving only 2D structure problem with weight 10^5.

Δt	L^2(w-function)
0.5	$1.43e-06$
0.25	$6.97e-07$[1.04]
0.125	$3.45e-07$[1.01]
0.0625	$1.73e-07$[1.00]
0.03125	$8.75e-08$[0.99]

where f_p is the function evaluated using manufactured w function. Another interesting point we noticed was the need for an even larger weight to achieve linear convergence in time with a smaller mesh size. This numerical finding suggests that errors are strongly dependent on a spatial mesh.

5.2 | Test 2: Free vibration of a plate

In this test, we examine a physical scenario involving the free vibration of a plate [32]. Consider the domains $\Omega_f = [0,1] \times [0,1] \times [-1,0]$ and $\Omega_p = [0,1] \times [0,1] \times \{0\}$, set $\mathbf{f}_f = 0$ and impose $\mathbf{u} = \mathbf{0}$ on all boundary faces of Ω_f, except at $z = 0$, where we have the condition $u_3 = w_t$. Additionally, at the boundary of the plate we set $w = \frac{\partial w}{\partial \mathbf{n}} = \frac{\partial w}{\partial t} = 0$. We use additional parameters and rewrite the plate structure as follows:

$$\rho_p w_{tt} - \rho \Delta w_{tt} + D\Delta^2 w = f_p \quad \text{in } \Omega_p \times (0,T),$$

where ρ_p is the density, $D := Yh^3/(12(1-\nu))$ is the flexural rigidity with ν and Y being the Poisson's ratio and Young's modulus, respectively. In this experiment we consider $\rho_p = 2.7, D = 6.4527$ and $\rho = 0$. By setting $D \neq 0$ and $f_p = \rho = 0$, the model reduces to the classical Kirchhoff-Love model with only the bending dynamics accounted. For the numerical experiment, we set mesh size $h = 1/12$, $T_{\text{final}} = 0.01$ seconds and $\tau = 0.001$ seconds. Initially, we set $\mathbf{u}(\mathbf{x}, 0) = \mathbf{0}, p(\mathbf{x}, 0) = 0$ and set the plate in the free vibration by introducing, for some integers m and n,

$$w_t(\mathbf{x}, 0) = \sin(m\pi x)\sin(n\pi y).$$

We plot u_3 in the fluid domain and w_t in the plate domain for different values of m and n. The plots in Figure 5 show that the vibration in the plate gets transmitted to the fluid dynamics, affecting the vertical velocity component of the fluid (u_3). Furthermore, we observed that the plot of w_t is the same as the standing wave solution mentioned in [32]. We also present the plot of u_3 for the $(m,n) = (1,2)$ case on the $x = 0.5$ plane (see Figure 6), which provides a clearer representation of u_3 in the fluid domain.

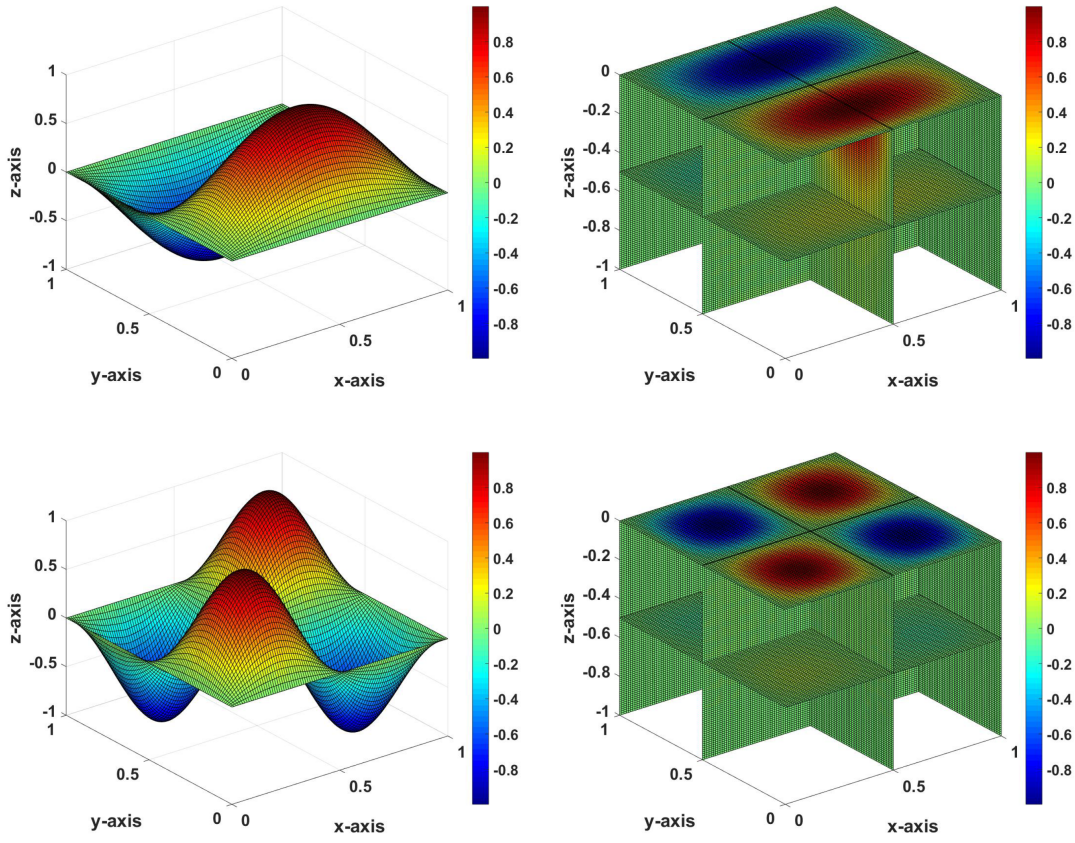

FIGURE 5 w_t(left) and u_3(right) for $h = 1/12$, $T_{\text{final}} = 0.01$, $\tau = 0.001$, $(m, n) = (1, 2)$ (top) and $(m, n) = (2, 2)$ (bottom).

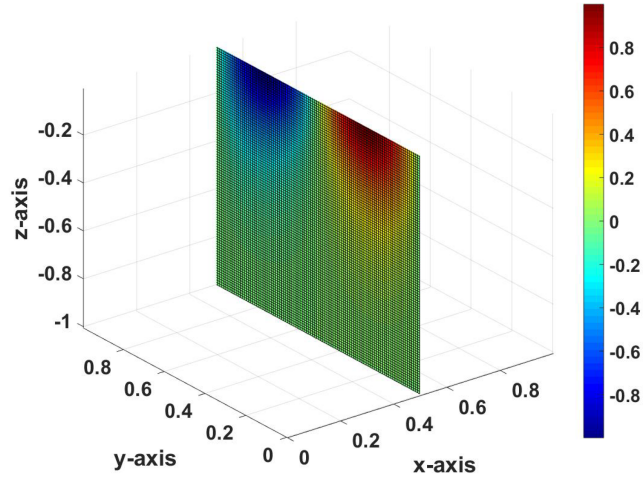

FIGURE 6 u_3 for $h = 1/12$, $T_{\text{final}} = 0.01$, $\tau = 0.001$ in $x = 0.5$ plane.

6 | CONCLUSION

We presented a second-order temporal numerical discretization scheme for the 3D fluid-2D plate structure interaction system and demonstrated its stability. Furthermore, we proposed a numerical algorithm that sequentially solves the fluid and plate subsystems through a decoupling approach. The numerical complexity arising from the biharmonic operator in the plate structure was addressed using $P2$Morley elements in the structure subproblem. The accuracy of the algorithm was demonstrated through the numerical results obtained from tests using time-dependent manufactured solutions and those considering the free vibration of the plate.

However, in the manufactured example, we did not observe second-order convergence in time because the errors remained consistently very small across various time step sizes. This observation motivates us to conduct further numerical studies on time discretization using different examples, including practical applications. Additionally, the limitation of numerical tests due to the large size of the fully discrete system may be addressed by employing a preconditioner for a linear solver, such as GMRES. In future work, the fluid-plate problem could be studied within a moving domain framework. This approach would involve considering a time-dependent fluid domain and utilizing a time-dependent bijective mapping, known as Arbitrary Lagrangian–Eulerian (ALE) mapping, to exchange information between the fixed reference domain and the physical domain.

FUNDING INFORMATION

Pelin G. Geredeli work was partially supported by the NSF under grant number DMS-2348312. Hemanta Kunwar and Hyesuk Lee work was partially supported by the NSF under grant number DMS-2207971.

DATA AVAILABILITY STATEMENT

The data that support the findings of this study are available from the corresponding author upon reasonable request.

ORCID

Hyesuk Lee https://orcid.org/0000-0002-6075-9735

REFERENCES

[1] M. Amara, C. Capatina-Papaghiuc, and A. Chatti, *Bending moment mixed method for the Kirchhoff-Love plate model*, SIAM J. Numer. Anal. 40 (2002), 1632–1649.
[2] G. Avalos and T. Clark, *Mixed variational formulation for the wellposedness and numerical approximation of a PDE model arising in a 3-D fluid-structure interaction*, Evol. Equ. Control Theory 3 (2014), no. 4, 557–578.
[3] G. Avalos and M. Dvorak, *A new maximality argument for a coupled fluid-structure interaction with implications for a divergence-free finite element method*, Appl. Math. 35 (2008), no. 3, 259–280.
[4] G. Avalos and R. Triggiani, *The coupled PDE System arising in fluid/structure interaction, Part I: Explicit semigroup generator and its spectral properties, Fluids and Waves*, AMS Contemp. Math. 440 (2007), 15–54.
[5] V. Barbu, Z. Grujić, I. Lasiecka, and A. Tuffaha, *Weak and strong solutions in nonlinear fluid-structure interactions, fluids and waves*, AMS Contemp. Math. 440 (2007), 55–82.
[6] V. Barbu, Z. Grujic, I. Lasiecka, and A. Tuffaha, *Smoothness of weak solutions to a nonlinear fluid-structure interaction model*, Indiana Univ. Math. J. 57 (2008), 1173–1207.

[7] A. Bermúdez, R. Rodríguez, and D. Santamarina, *Finite element computation of sloshing modes in containers with elastic baffle plates*, Int. J. Numer. Methods Eng. 56 (2003), no. 3, 447–467.

[8] T. Bodnar, G. P. Galdi, and S. Necasova, *Fluid-structure interaction and biomedical applications*, Birkhäuser/Springer, Basel, 2014.

[9] M. Bukac, S. Canic, and B. Muha, *A nonlinear fluid-structure interaction problem in compliant arteries treated with vascular stents*, Appl. Math.Opt. 73 (2016), no. 3, 433–473.

[10] E. Burman, R. Durst, and J. Guzmán, *Stability and error analysis of a splitting method using Robin-Robin coupling applied to a fluid-structure interaction problem*, Numer. Methods Partial Differ. Eq. 38 (2022), 1396–1406.

[11] A. Chambolle, B. Desjardins, M. J. Esteban, and C. Grandmont, *Existence of weak solutions for the unsteady interaction of a viscous fluid with an elastic plate*, J. Math. Fluid Mech. 7 (2005), 368–404.

[12] I. Chueshov and I. Ryzhkova, *A global attractor for a fluid-plate interaction model*, Commun. Pure Appl. Anal. 12 (2013), 1635–1656.

[13] P. G. Ciarlet and P. A. Raviart, "A mixed finite element method for the biharmonic equation," *Mathematical aspects of finite elements in partial differential equations*, Academic Press, New York, 1974, pp. 125–145.

[14] A. de Castro, H. Lee, and M. M. Wiecek. Formulation and analysis of a Schur complement method for fluid-structure interaction. arXiv preprint, arXiv:2304.15001v1 2023.

[15] Q. Du, M. D. Gunzburger, L. S. Hou, and J. Lee, *Analysis of a linear fluid-structure interaction problem, Discrete*, Cont. Dyn. 9 (2003), 633–650.

[16] D. Gallistl, *Morley finite element method for the eigenvalues of the biharmonic operator*, IMA J. Numer. Anal. 35 (2014), 1779–1811.

[17] K. J. Gavin, *New subgrid artificial viscosity Galerkin methods for the Navier-Stokes equations*, Comput. Methods Appl. Mech. Eng. 200 (2011), 242–250.

[18] C. Grandmont, *Existence of weak solutions for the unsteady interaction of a viscous fluid with an elastic plate*, SIAM J. Math. Anal. 40 (2008), 716–737.

[19] F. Hecht, *New development in freefem++*, J. Numer. Math. 20 (2012), 251–265.

[20] T. T. P. Hoang, H. Kunwar, and H. Lee, *Nonconforming time discretization based on Robin transmission conditions for the Stokes-Darcy system*, Appl. Math. Comput. 413 (2022), 126602.

[21] M. C. Hsu and Y. Bazilevs, *Blood vessel tissue prestress modeling for vascular fluid-structure interaction simulation*, Finite Elem. Anal. Des. 47 (2011), 593–599.

[22] R. A. Ibrahim, *Liquid sloshing dynamics: Theory and applications*, Cambridge University Press, Cambridge, 2005.

[23] C. Johnson, *On the convergence of a mixed finite-element method for plate bending problems*, Numer. Math. 21 (1973), 43–62.

[24] P. Kuberry and H. Lee, *A decoupling algorithm for fluid-structure interaction problems based on optimization*, Comput. Methods Appl. Mech. Eng. 267 (2013), 594–605.

[25] I. Kukavica, A. Tuffaha, and M. Ziane, *Strong solutions for a fluid-structure interaction system*, Adv. Differential Equ. 15 (2010), 231–254.

[26] H. Kunwar, H. Lee, and K. Seelman, *Second-order time discretization for a coupled quasi-Newtonian fluid-poroelastic system*, Int. J. Numer. Methods Fluids 92 (2020), 687–702.

[27] M. Li, X. Guan, and S. Mao, *New error estimates of the Morley element for the plate bending problems*, J. Comput. Appl. Math. 263 (2014), 405–416.

[28] O. Maklad, V. Theofilis, and A. Elsheikh, "*Fluid structure interaction (FSI) simulation of the human eye under the air puff tonometry using computational fluid dynamics (CFD)*," Tenth International Conference on computational fluid dynamics, Barcelona, Spain, July 9-13, 2018.

[29] S. Mao, S. Nicaise, and C. Z. Shi, *Error estimates of Morley triangular element satisfying the maximal angle condition*, Int. J. Numer. Anal. Model. 7 (2010), no. 4, 639–655.

[30] W. Ming and J. Xu, *The Morley element for fourth order elliptic equations in any dimensions*, Numer. Math. 103 (2006), 155–169.

[31] L. S. D. Morley, *The triangular equilibrium element in the solution of plate bending problems*, Aeronaut. Quart. 19 (1968), 149–169.

[32] D. T. A. Nguyen, L. Li, and H. Ji, *Stable and accurate numerical methods for generalized Kirchhoff-Love plates*, J. Eng. Math. 130 (2021), no. 1, 1–26.

[33] F. Nobile, *Numerical approximation of fluid-structure interaction problems with application to haemodynamics*, Ph.D. thesis, EPFL, Switzerland, 2001.

[34] J. Pestana, R. Muddle, M. Heil, F. Tisseur, and M. Mihajlovic, *Efficient block preconditioning for a C^1 finite element discretization of the Dirichlet biharmonic problem*, SIAM J. Sci. Comput. 38 (2016), A325–A345.

[35] R. Temam, *Navier-Stokes equations, theory and numerical analysis*, AMS Chelsea Publishing, Providence, RI, 2001.

[36] S. Zhang, *An optimal order multigrid method for biharmonic, C^1 finite element equations*, Numer. Math. 56 (1989), 613–624.

How to cite this article: P. G. Geredeli, H. Kunwar, and H. Lee, *Partitioning method for the finite element approximation of a 3D fluid-2D plate interaction system*, Numer. Methods Partial Differ. Eq. (2024), e23132. https://doi.org/10.1002/num.23132